



## Seeds of L<sub>12</sub> clusters in amorphous Mg<sub>85</sub>Zn<sub>6</sub>Y<sub>9</sub> alloy observed via anomalous X-ray scattering

Shinya Hosokawa<sup>1,2\*</sup>, Jens Rüdiger Stellhorn<sup>1,2</sup>, Benjamin Danilo Klee<sup>2</sup>, Wolf-Christian Pilgrim<sup>2</sup>, Hiroshi Okuda<sup>3</sup>, Michiaki Yamasaki<sup>4,5</sup>, Yoshihiro Kawamura<sup>4,5</sup>, Nils Blanc<sup>6,7</sup>, and Nathalie Boudet<sup>6,7</sup>

<sup>1</sup>Department of Physics, Kumamoto University, Kumamoto 860-8555, Japan

<sup>2</sup>Department of Chemistry, Physical Chemistry, Philipps University of Marburg, 35032 Marburg, Germany

<sup>3</sup>Department of Materials Science and Engineering, Kyoto University, Kyoto 606-8501, Japan

<sup>4</sup>Department of Materials Science, Kumamoto University, Kumamoto 860-8555, Japan

<sup>5</sup>Magnesium Research Center, Kumamoto University, Kumamoto 860-8555, Japan

<sup>6</sup>CNRS, Institut Néel, F-38000 Grenoble, France

<sup>7</sup>Université Grenoble Alpes, Institut Néel, F-38000 Grenoble, France

\*E-mail: shhosokawa@kumamoto-u.ac.jp

Received March 30, 2018; accepted May 28, 2018; published online June 14, 2018

An anomalous X-ray scattering experiment was performed on an amorphous Mg<sub>85</sub>Zn<sub>6</sub>Y<sub>9</sub> alloy. The experimental data were analyzed using a reverse Monte Carlo model to examine the existence of the seeds of Zn<sub>6</sub>Y<sub>8</sub> L<sub>12</sub> impurity clusters. The results reveal the highly enhanced existence of Zn–Y bonds rather than a random distribution of the impurities in the host Mg atoms. With respect to the theoretical structure of the clusters in the crystal phase, shorter nearest-neighboring Zn–Y and shorter second-neighboring Zn–Zn interatomic distances are observed as the fragments of the L<sub>12</sub> clusters. © 2018 The Japan Society of Applied Physics

In the past 15 years, novel Mg-based alloys containing Zn and rare-earth metal impurities<sup>1)</sup> have attracted considerable attention owing to their potential for widespread application as structural materials, as these alloys are lightweight compared with Al. The strength and ductility of pure Mg are very poor for applications. However, Mg alloys with small amounts of Zn and Y impurities exhibit superior mechanical properties, such as a tensile yield strength of ~600 MPa and the elongation of ~8% at room temperature.<sup>1,2)</sup> Moreover, pure Mg, which is flammable and chemically active, becomes non-flammable and exhibits high thermal stability<sup>2)</sup> after the addition of impurities. Because of such excellent properties, together with the ease of recycling, these Mg alloys are considered as next-generation structural materials, e.g., for bodies of subways or even aircrafts.

To clarify the origin of these remarkable properties from a structural viewpoint, extensive studies were performed using scanning transmission electron microscopy (STEM) and electron diffraction.<sup>3,4)</sup> According to these studies, a long-period stacking ordered (LPSO) phase is formed in the Mg alloys. The Mg<sub>85</sub>Zn<sub>6</sub>Y<sub>9</sub> alloy has a 18R-type (after the Ramsdell notation<sup>5)</sup>) LPSO structure with a volume fraction of up to ~100%,<sup>8)</sup> depending on the thermal history.<sup>4)</sup>

According to high-angle annular dark-field (HAADF) STEM observations performed by Abe et al.,<sup>6)</sup> which can reveal the chemical-sensitive Z-contrast, the Zn and Y impurities are enriched around the stacking faults. That is, the concentration of the impurity elements is synchronized with the stacking faults in the LPSO structure. For this reason, this curious structure is referred to as the synchronized LPSO phase.

Egusa and Abe<sup>7)</sup> reported that the characteristic ordered features of the 14H type for the Mg<sub>97</sub>Zn<sub>1</sub>Er<sub>2</sub> alloy and the 18R type for the Mg<sub>85</sub>Zn<sub>6</sub>Y<sub>9</sub> alloy are well-represented by local L<sub>12</sub> clusters, which are embedded in the face-centered cubic stacking layers. The existence of L<sub>12</sub>-type clusters was proposed by Shiraishi et al.<sup>8)</sup> in an Mg<sub>80.6</sub>Al<sub>8.3</sub>Gd<sub>11.1</sub> alloy,

where the crystal structure of the LPSO phase can be crystallographically described as one of the order–disorder structures, and by Yamasaki et al.<sup>9)</sup> in a highly ordered 10H-type LPSO phase in an Mg<sub>75</sub>Zn<sub>10</sub>Y<sub>15</sub> alloy.

Recently, Okuda et al. investigated the transformation process of amorphous-crystal phases in the Mg<sub>85</sub>Zn<sub>6</sub>Y<sub>9</sub> LPSO alloy using small-angle X-ray scattering.<sup>10)</sup> They observed a hierarchical transformation, where the clustering of the impurity atoms occurs first, and the spatial rearrangement of the clusters induces a secondary transformation leading to two-dimensional (2D) ordering of the L<sub>12</sub>-type Zn<sub>6</sub>Y<sub>8</sub> impurity clusters. In their manuscript, this process was clearly displayed to occur from the isolated impurities to the Zn<sub>6</sub>Y<sub>8</sub> L<sub>12</sub> clusters through the fragments of the clusters for the first process, and then the L<sub>12</sub> clusters are aligned to form the LPSO phase for the second one.

More recently, photoemission measurements were performed on amorphous Mg<sub>85</sub>Zn<sub>6</sub>Y<sub>9</sub> to investigate its chemical nature with the shift of the Y 3d core level.<sup>11)</sup> The most important result is that the 3d core spectrum exhibits three doublets in the amorphous phase. On the other hand, there is a single doublet in the crystalline phase, which fully originates from the atomic configurations of the L<sub>12</sub> clusters. The Y 3d binding energy of the crystalline phase coincides with that of the deepest one in the amorphous phase, with a large fraction of 57%. As we do not consider that more than half of the Y atoms can form the perfect Zn<sub>6</sub>Y<sub>8</sub> L<sub>12</sub> clusters, large fragments of the clusters are expected to have the same chemical nature.

To understand the formations of the Zn/Y impurity configurations in the amorphous phase, we performed anomalous X-ray scattering (AXS) experiments near the Zn and Y K absorption edges. The obtained data were analyzed using reverse Monte Carlo (RMC) modeling to draw three-dimensional (3D) atomic configurations around the impurity atoms, whereby the seeds of the L<sub>12</sub> clusters in the amorphous phase are discussed in detail.



An amorphous sample was manufactured at the Magnesium Research Center, Kumamoto University. Pure Mg (99.99 wt %), Zn (99.9 wt %), and Y (99.9 wt %) metals were mixed and melted using high-frequency induction a cylindrical C crucible in a pure Ar atmosphere and then rapidly quenched using a normal melt-spinning technique. The obtained amorphous ribbon was approximately 1 mm wide and 0.02 mm thick. The amorphous phase of the ribbon was examined via X-ray diffraction and transmission electron microscopy. The composition of the sample was confirmed to be a nominal value within 1 at. % using electron-probe microanalysis equipment.

The AXS experiments were performed at BM02 of the European Synchrotron Radiation Facility (ESRF) at the two energies of 20 and 200 eV below the Zn (9.659 keV) and Y (17.080 keV) K absorption edges. The measurements were performed in the transmission mode using a standard  $\omega$ - $2\theta$  diffractometer installed at the beamline. For discriminating the elastic signal from the  $K\beta$  fluorescent and Compton scattering contributions, a graphite crystal energy analyzer was mounted on a 1-m-long detector arm carrying a 2D detector. The feasibility of this detection system is described elsewhere.<sup>12,13)</sup> By employing the 2D detector, a stable experimental condition was achieved. Following the procedure given in the literature,<sup>12,14)</sup> differential structure factors,  $\Delta_k S(Q)$ , were obtained from the contrasts between diffraction data with different incident X-ray energies near each K edge of the  $k$  element. In the analysis, Sasaki's theoretical values<sup>15)</sup> were used for the anomalous terms.

RMC simulations<sup>16)</sup> were performed using  $\Delta_{Zn}S(Q)$ ;  $\Delta_Y S(Q)$ ; and the total structure factor, i.e.,  $S(Q)$ , to calculate partial structure factors,  $S_{ij}(Q)$ , and partial pair distribution functions,  $g_{ij}(r)$ , from which the 3D atomic configurations were deduced. The simulations were performed using the RMC++ program package coded by Gereben et al.<sup>17)</sup> with the scattering data of differently weighted  $S_{ij}(Q)$  values. The starting configurations of a system containing a total of 10,000 atoms were generated using hard-sphere Monte Carlo simulations, i.e., random configurations excluding short bonds. To avoid unphysical atomic configurations, the cut-off values were determined to be 0.25, 0.26, 0.26, 0.37, 0.25, and 0.37 nm for the Mg–Mg, Mg–Zn, Mg–Y, Zn–Zn, Zn–Y, and Y–Y atomic pairs, respectively. The original cut-off values were 0.25 nm for the all partials, and after the preliminary fits, very small contributions of the Zn–Zn and Y–Y impurity homopolar correlations were observed in the nearest-neighboring distance range. The cut-off distances were finally set as the aforementioned values.

The squares in Fig. 1 show the experimental results for  $\Delta_Y S(Q)$ ,  $\Delta_{Zn} S(Q)$ , and  $S(Q)$ , from top to bottom. The features of these structure factors appear very different from each other. First, the heights of the first peaks around  $0.24 \text{ nm}^{-1}$  in  $\Delta_k S(Q)$  of the impurity elements are smaller and their widths are broader than those of  $S(Q)$ . Second, the second peak and the subsequent shoulder in  $\Delta_{Zn} S(Q)$  differ significantly from the others. Third, the enhancement at low  $Q$  values is very sharp in  $\Delta_Y S(Q)$  compared with the others, indicating the formation of large clusters including the Y atoms. The solid curves in Fig. 1 indicate the best fits of the RMC modeling, which excellently coincide with the experimental structure factor data.

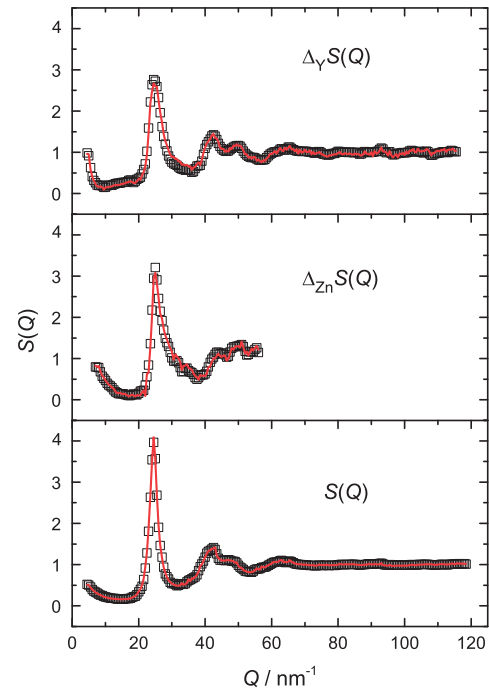


Fig. 1.  $\Delta_Y S(Q)$ ,  $\Delta_{Zn} S(Q)$ , and  $S(Q)$  for the amorphous  $\text{Mg}_{85}\text{Zn}_6\text{Y}_9$  alloy, from top to bottom. The squares represent the experimental results obtained via AXS, and the solid curves represent the RMC best fits.

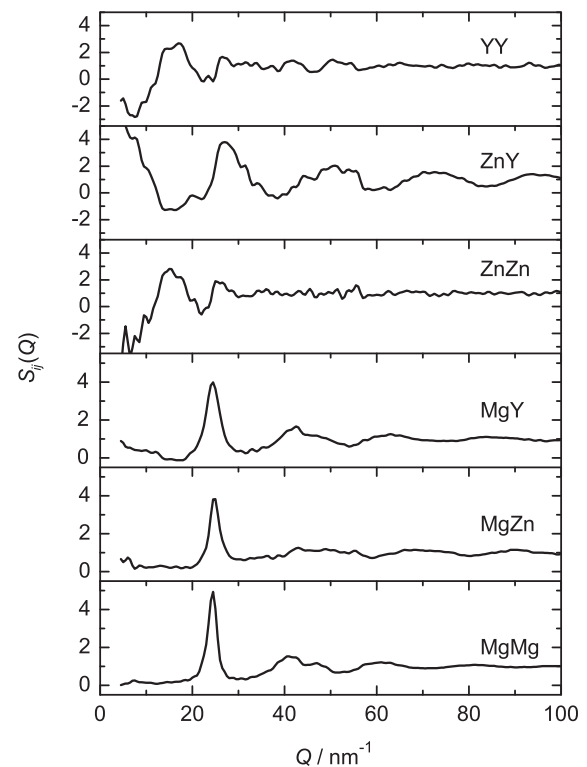
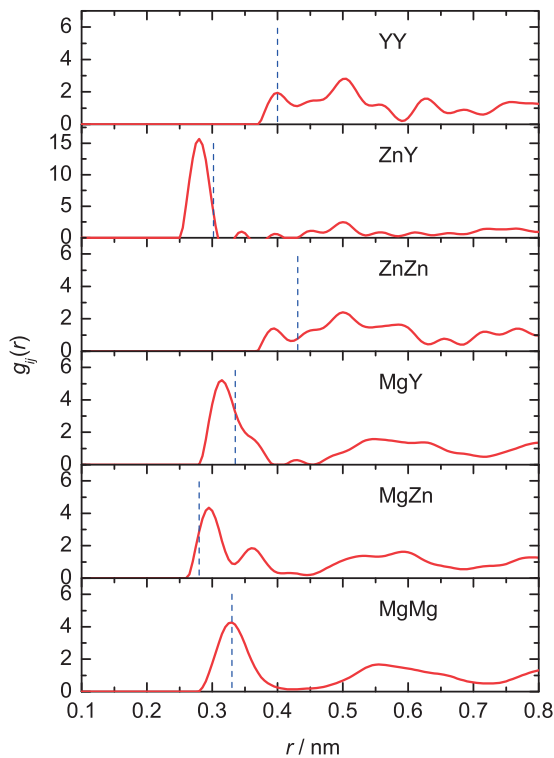


Fig. 2. The  $S_{ij}(Q)$  functions obtained from the RMC fits.

Figure 2 shows the  $S_{ij}(Q)$  functions obtained from the RMC fits. All of the Mg-related  $S_{ij}(Q)$  functions exhibit typical metallic glass-like features, where the prominent first peaks are located around  $23 \text{ nm}^{-1}$ . On the other hand, the Zn–Zn and Y–Y impurity homopolar partials exhibit broad first peaks at  $16$ – $17 \text{ nm}^{-1}$ , and the dampings are very prominent in the high- $Q$  range. Extremely different features are



**Fig. 3.** The  $g_{ij}(r)$  functions obtained from the RMC fits. The dashed lines indicate the interatomic distances in the crystal phase obtained via theoretical calculations.<sup>7)</sup>

observed for the Zn–Y impurity heteropolar partial, where the largest oscillations occur throughout the  $Q$  range and the enhancement is very large in the low- $Q$  range, indicating strong Zn–Y correlations and distinct Zn–Y cluster formations.

Figure 3 shows the  $g_{ij}(r)$  functions obtained from the RMC fits. The dashed lines indicate the interatomic distances in the crystal phase, which were obtained via theoretical calculations.<sup>7)</sup> The most prominent  $g_{ij}(r)$  function is found to be the Zn–Y partial, where the height of the first peak around 0.28 nm is larger than the others by a factor of three, indicating a strong Zn–Y interatomic correlation. The position of the Zn–Y first neighboring correlation is approximately 0.02 nm shorter in the amorphous phase than in the crystal. There are no correlations for the homopolar Zn–Zn and Y–Y partials in the first neighboring shell, as in the crystalline phase. The second peak around 0.50 nm is very large in both the Zn–Zn and Y–Y correlations, indicating the formation of the Zn/Y impurity clusters. The first-peak position around 0.40 nm in the Y–Y partial coincides well with that of the crystal phase, whereas that for Zn–Zn is shorter than that in the crystal and mostly matches the Y–Y first-peak position.

Concerning the Mg-related  $g_{ij}(r)$  functions, the Mg–Mg correlation exhibits typical metallic glass-like features, including a sharp first peak at the same  $r$  position as the crystal and a gradual second peak with a shoulder at the higher  $r$  positions. The first-peak positions in the Mg–impurity correlations differ from those for the crystal: they are longer in the Mg–Zn interatomic distance by approximately 0.015 nm and shorter in the Mg–Y one by approximately 0.030 nm. The spectra exhibit a peak or a shoulder at the higher  $r$  positions around 0.37 nm.

**Table I.** Partial coordination numbers and their fractions around the constituent elements.

	Mg (85%)	Zn (6%)	Y (9%)	Total
Mg	8.9 (84.8%)	0.6 (5.7%)	1.0 (9.5%)	10.5
Zn	8.3 (86.5%)	0	1.3 (13.5%)	9.6
Y	9.4 (91.3%)	0.9 (8.7%)	0	10.3

The partial coordination numbers,  $N_{ij}$ , were calculated using the RMC fit data. The maximum length for the Mg-related partials is defined to be 0.40 nm, where the first shell contains the Mg atoms. The maximum length between the impurity atoms was determined to be 0.33 nm, where only the Zn–Y first peak is contained. The results are shown in Table I. The total coordination number around each constituent element is approximately 10, which is significantly smaller than the dense-packed hcp Mg value of 12, indicating a sparse atomic configuration in the amorphous phase.

Around the host Mg atoms, the fractions of the partial coordination numbers mostly coincide with the nominal value of the atomic concentrations by less than 0.5%, indicating random configurations around the host Mg atoms. As mentioned previously, the Zn–Zn and Y–Y impurity homopolar interatomic correlations are not formed in the first neighboring shell. On the other hand, the Zn–Y and Y–Zn partial coordination numbers are significantly larger than the average values of the concentrations, by approximately 50%. Thus, the seeds of the  $Zn_6Y_8$   $L1_2$  clusters comprising the Zn–Y interatomic bonds are highly expected rather than random atomic configurations, even in the amorphous  $Mg_{85}Zn_6Y_9$  alloy.

To examine the atomic configurations around the Zn/Y impurity atoms in detail, we display the 3D atomic image in Fig. 4(a), which was obtained from the present RMC fit simulation. For clarity, the figure shows only a slab with a thickness of one-third of the simulation box. The Zn and Y impurity atoms are indicated by small and large balls, respectively, and the Mg atoms are removed for clarity. The bars indicate the first neighboring interatomic correlations with an interatomic length up to 0.33 nm between the Zn/Y impurity atoms.

For comparison, a random configuration is shown in Fig. 4(b), which was obtained via an RMC simulation with the same number density and cut-off lengths used in (a) but without any scattering data. As clearly shown in the figures, the AXS results in (a) comprise many large Zn/Y impurity clusters formed by Zn–Y bonds, while the random configuration comprises mostly isolated impurity atoms and a small number of accidentally formed Zn–Y bonds. Therefore, the analysis of the AXS results using RMC modeling indicates that the seeds of the  $Zn_6Y_8$   $L1_2$  clusters are already prepared in the amorphous  $Mg_{85}Zn_6Y_9$  alloy with large sizes, which is consistent with the previous Y 3d core-level photoemission measurements.<sup>11)</sup>

Here, a question arises: why do the obtained clusters in Fig. 4 appear chain-like rather than exhibiting a spherical shape similar to the  $L1_2$  clusters in the crystal? To answer this, the algorithm of the RMC simulation should be considered. The RMC calculation attempts to fit the atomic arrangements to the experimental data without considering the energy landscape of atomic configurations. During the simulation, atoms move randomly; thus, the entropy of the

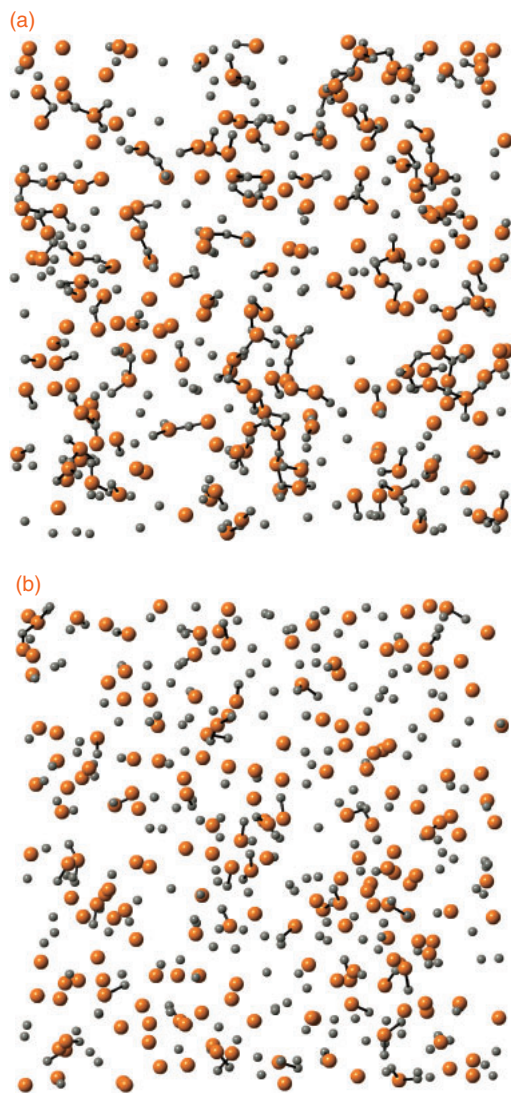


**Fig. 4.** 3D atomic configurations of Zn and Y impurities indicated by small and large balls, respectively. (a) AXS results and (b) a random configuration. The bars indicate the first neighboring interatomic correlations with an interatomic length up to 0.33 nm between the Zn/Y impurity atoms. The Mg atoms are removed for clarity.

system is the driving force within the framework of the scattering data. Therefore, to maximize the entropy of the system, the RMC algorithm strongly prefers chain-like configurations over spherical ones.

There was a serious controversy regarding the structure of phosphate glass, i.e., the fraction of the boroxol  $B_2O_3$  rings in the glass. Using nuclear magnetic resonance, which is a sensitive technique for determining the local structure in glasses, it was concluded that the fraction of B atoms in boroxol rings,  $f$ , exceeds 75%,<sup>18)</sup> which was also observed in highly resolved inelastic neutron scattering spectra.<sup>19)</sup> In contrast, RMC results obtained using a combination of X-ray and neutron scattering data show a small  $f$  value of < 20%.<sup>20,21)</sup> Details regarding this argument are provided elsewhere.<sup>22)</sup> The boroxol ring is a low-entropy configuration rather than its fragment of the B–O chain; thus, it is highly

possible that the  $f$  value obtained via RMC is significantly underestimated owing to the simulation algorithm. Therefore, the formation of the sphere-like clusters cannot be excluded in the present RMC results.

An AXS experiment was performed on an amorphous  $Mg_{85}Zn_6Y_9$  alloy. The experimental data were analyzed using an RMC model to examine the existence of the seeds of  $Zn_6Y_8$   $L1_2$  impurity clusters, which are aligned along the stacking faults in the crystalline phase. The results reveal a highly enhanced existence of Zn–Y bonds rather than a random distribution of the impurities in the host Mg atoms, which was discussed in relation to the triple sites in the Y 3d core-level photoemission spectra.<sup>11)</sup> With respect to the theoretical structure of the clusters, shorter nearest-neighboring Zn–Y and shorter second-neighboring Zn–Zn interatomic distances are observed in the fragments of the  $L1_2$  clusters.

**Acknowledgments** The AXS experiment was performed at BM02 of the ESRF (Proposal Nos. HC3144, HC3146, and HC3438). The supporting experiments were performed at BL13XU of SPring-8 (Proposal Nos. 2016B1192 and 2017B1201). This work was supported by a Grant-in-Aid for Scientific Research on Innovative Areas “Materials Science on Synchronized LPSO Structure” (No. 26109716) from the Japan Society for the Promotion of Science (JSPS). JRS gratefully acknowledges financial support obtained as an Overseas Researcher under a JSPS fellowship (No. P16796).

- 1) Y. Kawamura, K. Hayashi, A. Inoue, and T. Masumoto, *Mater. Trans.* **42**, 1172 (2001).
- 2) Y. Kawamura, T. Kasahara, S. Izumi, and M. Yamasaki, *Scr. Mater.* **55**, 453 (2006).
- 3) K. Hagihara, A. Kinoshita, Y. Sugino, M. Yamasaki, Y. Kawamura, H. Y. Yasuda, and Y. Umakoshi, *Acta Mater.* **58**, 6282 (2010).
- 4) M. Yamasaki, K. Hagihara, S. Inoue, J. P. Hadorn, and Y. Kawamura, *Acta Mater.* **61**, 2065 (2013).
- 5) L. S. Ramsdell, *Am. Mineral.* **32**, 64 (1947).
- 6) E. Abe, A. Ono, T. Itoi, M. Yamasaki, and Y. Kawamura, *Philos. Mag. Lett.* **91**, 690 (2011).
- 7) D. Egusa and E. Abe, *Acta Mater.* **60**, 166 (2012).
- 8) K. Shiraiishi, T. Mayama, M. Yamasaki, and Y. Kawamura, *Mater. Sci. Eng. A* **672**, 49 (2016).
- 9) M. Yamasaki, M. Matsushita, K. Hagihara, H. Izuno, E. Abe, and Y. Kawamura, *Scr. Mater.* **78–79**, 13 (2014).
- 10) H. Okuda, M. Yamasaki, Y. Kawamura, M. Tabuchi, and H. Kimizuka, *Sci. Rep.* **5**, 14186 (2015).
- 11) S. Hosokawa, J. R. Stellhorn, B. Paulus, K. Maruyama, K. Kobayashi, H. Okuda, M. Yamasaki, Y. Kawamura, and H. Sato, *J. Alloys Compd.* (in press) [DOI: 10.1016/j.jallcom.2018.06.012].
- 12) S. Hosokawa, Y. Wang, J.-F. Bézar, J. Greif, W.-C. Pilgrim, and K. Murase, *Z. Phys. Chem.* **216**, 1219 (2002).
- 13) S. Hosokawa, W.-C. Pilgrim, J.-F. Bézar, and S. Kohara, *Eur. Phys. J.: Spec. Top.* **208**, 291 (2012).
- 14) S. Hosokawa, I. Oh, M. Sakurai, W.-C. Pilgrim, N. Boudet, J.-F. Bézar, and S. Kohara, *Phys. Rev. B* **84**, 014201 (2011).
- 15) S. Sasaki, KEK Rep. 88-14 (1989).
- 16) R. L. McGreevy and L. Pusztai, *Mol. Simul.* **1**, 359 (1988).
- 17) O. Gereben, P. Jávári, L. Temleitner, and L. Pusztai, *J. Opt. Adv. Mater.* **9**, 3021 (2007).
- 18) R. E. Youngman and J. W. Zwanziger, *J. Non-Cryst. Solids* **168**, 293 (1994).
- 19) A. C. Hannon, D. I. Grimley, R. A. Hulme, A. C. Wright, and R. N. Sinclair, *J. Non-Cryst. Solids* **177**, 299 (1994).
- 20) J. Swenson and L. Börjesson, *Phys. Rev. B* **55**, 11138 (1997).
- 21) K. Suzuya, Y. Yoneda, S. Kohara, and N. Umesaki, *Phys. Chem. Glasses* **41**, 282 (2000).
- 22) S. Hosokawa, H. Sato, K. Mimura, Y. Tezuka, D. Fukunaga, K. Shimamura, and F. Shimojo, *J. Phys. Soc. Jpn.* **83**, 114601 (2014).